Robust gamma oscillations in networks of inhibitory hippocampal interneurons

P H E Tiesinga†‡§ and Jorge V José†

† Center for Interdisciplinary Research on Complex Systems, and Department of Physics, Northeastern University, 360 Huntington Avenue, Boston, MA 02115, USA
‡ Sloan Center for Theoretical Neurobiology, Salk Institute, 10010 N Torrey Pines Road, La Jolla, CA 92037, USA

E-mail: tiesinga@salk.edu

Abstract. Recent experiments suggest that inhibitory networks of interneurons can synchronize the neuronal discharge in *in vitro* hippocampal slices. Subsequent theoretical work has shown that strong synchronization by mutual inhibition is only moderately robust against neuronal heterogeneities in the current drive, provided by activation of metabotropic glutamate receptors. *In vivo* neurons display greater variability in the interspike intervals due to the presence of synaptic noise. Noise and heterogeneity affect synchronization properties differently. In this paper we study, using model simulations, how robust synchronization can be in the presence of synaptic noise and neuronal heterogeneity. We find that stochastic weak synchronization (SWS) (i.e. when neurons spike within a short interval from each other, but not necessarily at each period) is produced with at least a minimum amount of noise and that it is much more robust than strong synchronization (i.e. when neurons spike at each period). The statistics produced by the SWS population discharge are consistent with previous experimental data. We also find robust SWS in the gamma-frequency range (20–80 Hz) for a stronger synaptic coupling compared with previous models and for networks with 10–1000 neurons.

1. Introduction

One of the important properties of the behaviour of the nervous system is the synchronization of neuronal discharges. It was discovered early on [1], and it has attracted a significant amount of attention. In recent years the advent of improved experimental techniques has provided vast amounts of new synchronization data. Concomitantly, there has been a resurgence in interest and controversy concerning the functional relevance of synchronization. It has been established that *in vivo* cortical neurons have noisy spike trains [2] (see also [3]), and that groups of neurons discharge coherently, as found in population recordings (such as EEGs, or by arrays of extracellular electrodes; for a review see [4]). These two facts have sparked major controversies. Firstly, does noise (or precise timing) in neuronal spike trains contain information [5, 6], or is information merely due to noisy processing of an average firing rate [7–9]? Secondly, is synchronization functionally (or even statistically) significant [10, 11], or just an epiphenomenon [9]? In this paper we focus on two different aspects of synchronization that have received little attention so far. Can realistic neuronal networks synchronize under the biological conditions of variable intrinsic neuronal properties,

§ Author to whom correspondence should be addressed.

and the noise-induced neuronal unreliability? What kind of synchronization can be obtained, and what are its pertinent statistical properties? It is necessary to resolve these two questions to properly formulate the issues to be studied in experiment, and to analyse different ways of probing the experimental data. Here we focus our attention on the extensively studied synchronous gamma oscillations in hippocampus [12–17]. Theoretical and computational work has shown that mutual inhibition is capable of synchronizing neuronal networks [18,19]. Subsequent *in vitro* experiments have convincingly established the role of GABA-ergic hippocampal interneurons in gamma oscillations [12, 14]. Wang and Buzsáki studied the effect of current heterogeneity and partial connectivity on the synchronization of the inhibitory network [20]. They only found strong synchronization in the gamma-frequency range when the current heterogeneities were small [20–22]. In strong synchronization all neurons in a local circuit spike within a short interval of each other. This suggests that strong synchronization can only be obtained when the intrinsic properties of the neurons are not too different. According to [20] this would mean a less than 10% difference in current drive, or average firing rate. It has been hard to pinpoint the amount of variability in intrinsic properties in the *in vitro* and *in vivo* preparations of different brain areas. It is, however, not unreasonable to assume the presence of more than 10% variability in these preparations. Strong synchronization is also not robust against noise [22]. It would therefore seem unlikely for strong synchronization to be present in hippocampus under physiological conditions. Indeed, here we show that stochastic weak synchronization (SWS) is more prevalent in parameter space, and is also robust against neuronal heterogeneities and synaptic noise. We conjecture that as a consequence it is much more likely to occur in neuronal systems.

In SWS, neurons spike within a short interval from each other, but not necessarily at each period [23–25]. The synchronization is called stochastic, because the particular cycle in which the neurons fire is random. This makes the properties of this state different from the well known cluster states studied by previous authors [26–29]. There each neuron always fires at the same cycle with the same cluster. Both strong and stochastic weak synchronization yield periodic population oscillations. The difference can then be ascertained using multi-unit recordings.

We use cross correlation analysis to show that noise and heterogeneity affect the synchronization properties of our network in very different ways. Large enough noise and heterogeneity will, however, stop strongly synchronized oscillations. We demonstrate that increasing synaptic coupling does not significantly increase robustness of strong synchronization. We then determine for what parameters robust self-induced 40 Hz synchronous oscillations can be obtained. Finally, we compare the effects on synchronization of weak and strong synaptic coupling in a single neuron driven by a simulated network input.

2. Methods

2.1. Neuron models

Our aim here is to establish physiological criteria for robust synchronization in the gamma-frequency range. The use of a biophysically realistic model is therefore of pivotal importance, trying to balance the amount of complexity versus practical simplicity [30]. We have therefore not attempted to use the latest available data to construct the most detailed multi-compartmental model. If we tried to do so, the computer requirements to sample the full relevant parameter space, and perform our type of analysis, would be extremely demanding even using the fastest computers. It has been shown, nonetheless, that one and two compartmental models can accurately generate spike trains of the right shape and frequency [31–33]. Multi-compartmental models may be necessary, however, to assess the synaptic integration of inputs

located on different parts of the dendritic tree. This is currently an intensely studied area in electrophysiology [34–36]. Here we study a model previously introduced by others [20]. The model has been shown to reproduce the salient features of the dynamics of hippocampal interneurons. The neurons are modelled as a single compartment with Hodgkin–Huxley-type sodium and potassium channels. In this work all the neurons are connected all to all, and to themselves via inhibitory GABA$_A$-synapses. The equation for the membrane potential of a neuron is (the index i of the ith neuron is omitted)

$$C_m \frac{\mathrm{d}V}{\mathrm{d}t} = -I_{Na} - I_K - I_L - I_{\text{syn}} + I + C_m\xi. \tag{1}$$

Here we use the leak current $I_L = g_L(V - E_L)$ the sodium current $I_{Na} = g_{Na}m_\infty^3 h(V - E_{Na})$, the potassium current $I_K = g_K n^4(V - E_K)$, and the synaptic current $I_{\text{syn}} = g_{\text{syn}}s(V - E_{\text{syn}})$. The Gaussian noise variable is denoted as ξ (see below), and I is the tonic drive. The channel kinetics are given in terms of m, n, and h. They satisfy the following first-order kinetic equations,

$$\frac{\mathrm{d}x}{\mathrm{d}t} = \zeta(\alpha_x(1 - x) - \beta_x x). \tag{2}$$

Here x labels the different kinetic variables m, n, and h, and $\zeta = 5$ is a dimensionless timescale that can be used to tune the temperature-dependent speed with which the channels open or close. The rate constants are [20],

$$\alpha_m = \frac{-0.1(V + 35)}{\exp(-0.1(V + 35)) - 1},$$
$$\beta_m = 4\exp(-(V + 60)/18),$$
$$\alpha_h = 0.07\exp(-(V + 58)/20),$$
$$\beta_h = \frac{1}{\exp(-0.1(V + 28)) + 1},$$
$$\alpha_n = \frac{-0.01(V + 34)}{\exp(-0.1(V + 34)) - 1},$$
$$\beta_n = 0.125\exp(-(V + 44)/80).$$

We make the approximation that m follows the asymptotic value $m_\infty(V(t)) = \alpha_m/(\alpha_m + \beta_m)$, instantaneously. The synaptic gating variable s obeys the following equation [20, 37, 38]:

$$\frac{\mathrm{d}s}{\mathrm{d}t} = \alpha F(V_p)(1 - s) - \beta s, \tag{3}$$

with $\alpha = 12$ ms^{-1}, $\beta = 1/\tau_{\text{syn}}$, $F(V_p) = 1/(\exp(-V_p/2) + 1)$, and V_p is the presynaptic potential. The function $F(V_p)$ is chosen such that when the presynaptic neuron fires, $V_p > 0$, the synaptic channel opens. The decay time of the postsynaptic hyperpolarization is chosen as $\tau_{\text{syn}} = 1/\beta = 10$ ms (or 20 ms in some instances). We use a reversal potential of $E_{\text{syn}} = -75$ mV for the inhibitory (GABA$_A$) synapses [39]. The standard set of values for the conductances used in this work is $g_{Na} = 35$, $g_K = 9$, $g_L = 0.1$, and $g_{\text{syn}} = 0.1$ (in mS cm^{-2}), and we have taken $E_{Na} = 55$ mV, $E_K = -90$ mV, and $E_L = -65$ mV. The membrane capacitance is $C_m = 1\mu$F cm^{-2}. Unless stated otherwise we will use the standard set of parameters listed above. When no current value is specified we use $I = 1$ μA cm^{-2}. The network will then spike at approximately 39 Hz.

We chose the initial values for the membrane potential at the start of the simulations uniformly random between -70 and -50 mV. The kinetic variables m, n, h, and s are set to their asymptotic stationary values corresponding to that starting value of the membrane potential.

The resulting equations with noise are integrated using an adapted second-order Runge–Kutta method [40], with time step $dt = 0.01$ ms. The accuracy of this integration method was checked for the dynamical equations without noise ($D = 0$) by varying dt and comparing the result with the one obtained with the standard fourth-order Runge–Kutta method [41] with a time-step dt of 0.05 ms.

We normalize all quantities by the surface area of the neuron. This leads to the following system of units: the membrane potential V in mV, time t in ms, firing rate f in Hz, membrane capacitance C_m in μF cm^{-2}, conductance g_x in mS cm^{-2}, voltage noise ξ in mV ms^{-1}, strength of neuroelectric noise D in mV^{-2} ms^{-1}, the rate constants α_x and β_x in ms^{-1}, and the current I in μA cm^{-2}. The kinetic variables m, n, h, s, and the timescale ζ are dimensionless. The results in this paper are expressed in this system of units.

2.2. Heterogeneity and synaptic noise

We have included heterogeneity in the applied current. The current heterogeneity represents the variation in the intrinsic properties of the neurons in the hippocampus. For each run we draw the applied current for each neuron from a uniform probability distribution, with average current I and with variance σ_I^2. Experimental measurements of quantities like the input resistance R_{in}, the membrane timescale, the spontaneous spiking rate, the shape of the somatic action potential (amplitude, width, rise and fall time), and the afterhyperpolarization, show considerable variance [42–44]. It is hard to determine how much of the variance is due to measurement errors, and how much it is actually due to intrinsic neuronal variability. Here we assume that the main effect of the variability is to change the intrinsic frequency of the neurons (which can be varied using the current drive in our model). Another source of heterogeneity in *in vitro* experiments is the glutamate pressure ejection method [14]. It can lead to an inhomogeneous activation of metabotropic glutamate receptors, and thus to a variable current. In this paper we will consider σ_I as a free parameter.

At least three sources of noise can be identified [45]: (i) random inhibitory postsynaptic potentials (IPSP) and excitatory postsynaptic potentials (EPSP), (ii) stochasticity of the synaptic transmission, and the (iii) stochasticity of the channel dynamics. Here we assume that the variability in the neuronal discharge is mainly due to synaptic noise [46]. We have compared the effects of Poisson distributed spike trains of EPSPs and IPSPs with that of a Gaussian noise current on interspike interval (ISI) variability. Poisson and Gaussian noises do not yield identical results. The statistics obtained from both models, however, are similar in the parameter regime studied here [47]. For the purpose of our studies we consider that Poisson and Gaussian distributions are two alternate ways of producing noisy spike trains with particular statistics. Therefore, we consider only Gaussian synaptic noise ξ_i in the current of each neuron i, with $\langle \xi_i(t) \rangle = 0$, and $\langle \xi_i(t)\xi_j(t') \rangle = 2D\delta(t - t')\delta_{ij}$. The noise currents in different neurons are assumed independent.

2.3. Calculated quantities

From our simulations we obtain the time trace for the membrane potential $V_i(t)$ of each neuron. We determine the spike-trace X_i from V_i as follows: $X_i(t) = 1$ when $V_i(t)$ crosses 0 mV (i.e. $V(t^-) \leqslant 0 < V(t^+)$), and it is zero elsewhere. From X_i we obtain $X(t) = \sum_i X_i(t)$. X is proportional to the instantaneous firing rate of the network. We also calculate the coherence

function κ [20]:

$$\kappa \equiv \sum_{i \neq j} \frac{\langle \hat{X}_i(n\tau) \hat{X}_j(n\tau) \rangle}{\sqrt{\langle \hat{X}_i(n\tau) \rangle \langle \hat{X}_j(n\tau) \rangle}}. \tag{4}$$

This function measures the amount of strong synchronization, and depends on the bin size τ of the time discretization

$$\hat{X}_i(n\tau) = \sum_{(n-1)\tau \leqslant s < n\tau} X_i(s). \tag{5}$$

In this expression we rebin the original X_i into larger bins τ. We use $\tau = 200 \, \mathrm{d}t = 2$ ms for oscillations in the gamma-frequency range, or $T/10$ for periodic drives with period T.

We also calculate the time autocorrelation function

$$g_x(t) = \frac{\langle x(t)x(0) \rangle - \langle x \rangle^2}{(\langle x^2 \rangle - \langle x \rangle^2)}, \tag{6}$$

and the cross correlation function

$$g_{xy}(t) = \frac{\langle x(t)y(0) \rangle - \langle x(t) \rangle \langle y(0) \rangle}{\sqrt{\langle x(t)^2 \rangle \langle y(0)^2 \rangle}}. \tag{7}$$

Here x and y can be any of the variables X_i, V_i, and X. $\langle \, \rangle$ is a shorthand notation for the time average, in particular,

$$\langle x(n\tau)x(0) \rangle = \frac{1}{N - n_{\max}} \sum_{i=0}^{N-n_{\max}-1} x(i\tau)x((\mathrm{i}+n)\tau). \tag{8}$$

Here $x(n\tau)$ is the discretized variable obtained from the simulations ($\tau = 20 \, \mathrm{d}t = 0.2$ ms), $n_{\max} = 499$ is the maximum difference for which the cross correlations are evaluated, N is the number averaging steps. We evaluate these quantities since they yield further detailed quantitative characterization of the network behaviour.

We also consider the more conventional interspike interval histogram (ISIH) [48], averaged over all network neurons. From the ISIH one can obtain two statistics: the average ISI, τ_{ISI}, and the standard deviation of the ISI, σ_{ISI}. The ratio $\sigma_{\mathrm{ISI}}/\tau_{\mathrm{ISI}}$ is known as the coefficient of variation (CV). The average firing rate is $f = 1/\tau_{\mathrm{ISI}}$, and the population standard deviation of f is σ_f:

$$\sigma_f = \sum_j f_j^2 - f^2, \tag{9}$$

where $f_j = 1/\tau_{\mathrm{ISI}}^j$ is the average firing rate of the jth neuron. In addition, we plot rastergrams, with the action potential of each neuron plotted as a filled circle, with the y-coordinate given by the neuron index and the x-coordinate by the spiking time.

To analyse the stochastic weak synchronization network dynamics we need to apply a different method. In figure 1 we illustrate the various quantities that are introduced and defined below. The population period τ_n is different from the population averaged ISI, and to estimate it we proceed as follows. First we determine the firing rate $\hat{X}(t)$ as before in 1 ms bins. In the stochastic weak synchronization state $\hat{X}(t)$ will consist of a number of approximately equidistant peaks of finite width. We use the position of the first maximum at nonzero frequency in the Fourier transform, to obtain an estimate T for the period τ_n. We calculate the weight or cluster size $N_c^i = \langle \hat{X}(t) \rangle$, the average position $t_c^i = \langle t\hat{X}(t) \rangle / N_c^i$, and the width $\sigma_c^i = \sqrt{\langle t^2 \hat{X}(t) \rangle / N_c^i - (t_c^i)^2}$ of the ith peak. The time average $\langle \cdot \rangle$ is taken over a range $[-0.35T, 0.35T]$ about the estimated position $t_c^{i-1} + T$ of the peak. We calculated the
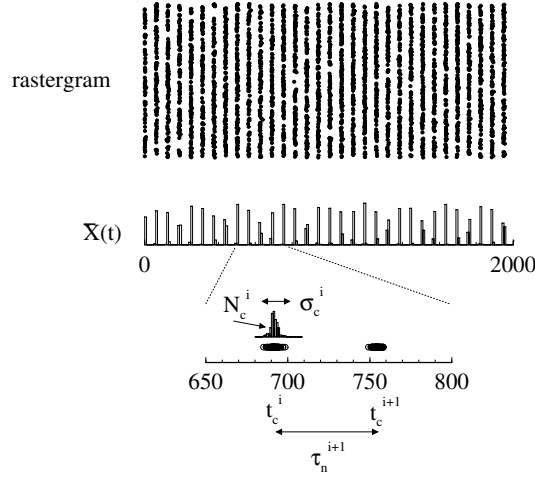
Figure 1. Definition of the parameters characterizing the SWS state. Here we show illustrative results for the statistical quantities introduced in the methods section using data from an example of a weakly synchronized state. From top to bottom we plot a rastergram, the corresponding instantaneous firing rate and its close-up. A cluster in a given cycle i is characterized by the average spike time t_c^i, the number of spikes N_c^i, and the standard deviation, σ_c^i, of spike times. The instantaneous cycle period τ_n^{i+1} is the difference in consecutive average spike times. As is explained in the text, the average over all cycles of N_c^i, σ_c^i, and τ_n^i are denoted as N_c, σ_c, and τ_n, respectively.

number of spikes that fall outside this region. If the average number of missed spikes is more than one per cycle we reject the cluster state. The instantaneous cycle length (the time between two consecutive cluster firings) is defined as $\tau_n^{i+1} = t_c^{i+1} - t_c^i$. We determine the average cluster size $N_c = \langle N_c^i \rangle$, its $CV(N_c) = \sqrt{\langle (N_c^i)^2 \rangle - N_c^2}/N_c$, the average cycle length $\tau_n = \langle \tau_n^i \rangle$, its $CV(\tau_n) = \sqrt{\langle (\tau_n^i)^2 \rangle - \tau_n^2}/\tau_n$, and the average width $\sigma_c = \langle \sigma_c^i \rangle$. Here the average $\langle \cdot \rangle$ is given by the sum over all cycles in the run (after discarding a transient).

We characterize the strength of the synchronization using a modified κ_W and CV_W (see below), where W stands for weak. In the SWS state the ISIH has multiple peaks. The CV of the ISI receives contributions from the variance within each peak, and also of the variance between the multiple peaks. We are only interested in the former, and the conventional CV is thus an overestimate. Instead we use

$$CV_W = \sigma_c/\tau_n, \tag{10}$$

which is related to the average width of one peak in the ISIH. (Note that for a constant instantaneous firing rate $CV_W = 1/\sqrt{12} \approx 0.29$.) The coherence κ measures the number of coincident spikes between two spike trains. Consider two neurons that do not spike at each cycle, but when they both do, the spikes are coincident (that is in the same bin). If the probability of spiking in a cycle is $p = N_c/N$, and both neurons fire statistically independent, we obtain $\kappa = p$ in (4). These neurons can be considered synchronous and we want $\kappa = 1$. We therefore normalize κ by p, and denote it as κ_W to indicate this fact:

$$\kappa_W = \kappa \frac{N}{N_c}. \tag{11}$$

There is a subtlety in the calculation of the average firing rate. In the deterministic noiseless case one ISI is enough to determine the average value (after discarding the transient). (Note that counting the number of spikes in a fixed interval is not an efficient way to determine

the exact firing rate.) In the presence of noise, however, we need to have, say at least ten ISIs to accurately determine the ensemble average properties of the random model, where the randomness comes from the noise. In networks with large current heterogeneities there are neurons with high and very low firing rates (figure 12). The average ISI for the low firing rate is less accurate than for the high firing rate neurons in the network. However, it carries equal weight in the conventional average $\tau_{\text{ISI}} = \sum_j \tau_{\text{ISI}}^j$. We have therefore used a weighted average $\tau_{\text{ISI}} = \sum_j n_j \tau_{\text{ISI}}^j / \sum_j n_j$ (here n_j is the number of intervals over which τ_{ISI}^j is calculated), and the approximate identity $N_c/\tau_n \approx N_s/\tau_{\text{ISI}}$ can be used as a check. N_s is the number of active neurons, defined as the neurons that have more than two ISIs after the transient.

We have also studied the behaviour of a single neuron driven by a simulated network input with period T. We define the phase of the nth output spike at time t_n as $\phi_n = t_n/T \mod 1$. The average $\langle \cdot \rangle$ over all spikes is then $\phi = \langle \phi_n \rangle$, and the standard deviation $\sigma_\phi = \sqrt{\langle \phi_n^2 \rangle - \phi^2}$. σ_ϕ is the single neuron equivalent of CV_W. The network input is applied at phase $\phi = \frac{1}{2}$.

3. Results

3.1. Non-robustness of strong synchronization

In this section we describe the results of our simulations for a network of $N = 100$ interneurons, connected all to all, with either synaptic noise (SN), or current heterogeneities (CH). In figure 2 we plot the coherence parameter κ (defined in (4)) versus the strength of the synaptic noise D, and versus the standard deviation of the current heterogeneities σ_I. We find that strong synchronization is lost for approximately $D > 0.10 \text{ mV}^2 \text{ ms}^{-1}$ and $\sigma_I > 0.1 \mu\text{A cm}^{-2}$ (with the standard set of parameters listed in the methods section). The mechanism by which strong synchronization is lost, however, is different in the CH case compared with the mechanism with SN. This difference shows up only if we study the whole state of the network using cross correlation functions, instead of the average quantities shown in figure 2. Wang and Buzsaki [20] (in what follows we refer to this reference as WB) have already analysed the case with current heterogeneity. We have reproduced part of their work, and we will refer to their corresponding figures. In both CH and SN cases the neuronal firing rate decreases when the network desynchronizes. We have plotted the time-trace of the synaptic drive $s(t)$ in figures 2(c) and (d). The phasic part decreases, and the tonic part of $s(t)$ increases with increasing D and σ_I. The increased tonic part is responsible for the lower average firing rate. The firing rate of the CH neurons saturates (when averaged over enough realizations of the current heterogeneities†), whereas for the SN it increases steadily as a function of D for large values of D. The single-neuron firing rate increases with D [47], but tonic inhibition saturates to its highest value in the asynchronous network. The dispersion σ_f (see the methods section) with CH is larger than the one in SN (not shown). In SN all neurons have identical intrinsic properties, and the expectation value for the average frequency of each neuron is the same. The dispersion σ_f in this case represents the fluctuations in the average ISI due to the finite averaging time. With CH the neurons have different intrinsic frequencies, and the dispersion σ_f increases with σ_I (and does not go to zero after a long averaging time; see WB figure 5B). In figures 3(I) and (II) we compare the correlation functions for the SN and CH cases, respectively. In (a) we have the strongly synchronous network, in (c) the asynchronous network, and in (b) a transition state. The difference between SN and CH becomes clear when one considers the cross correlation functions. With CH the number of pairs that are phase locked drops gradually (see WB figure 8E). The pairs that are phase locked, are tightly phase locked (figure 3I(b)1,

---

† This assumes $\int_{I_{av}-\sigma_I\sqrt{12}}^{I_{av}+\sigma_I\sqrt{12}} f(I) \, dI \approx f(I_{av})$.
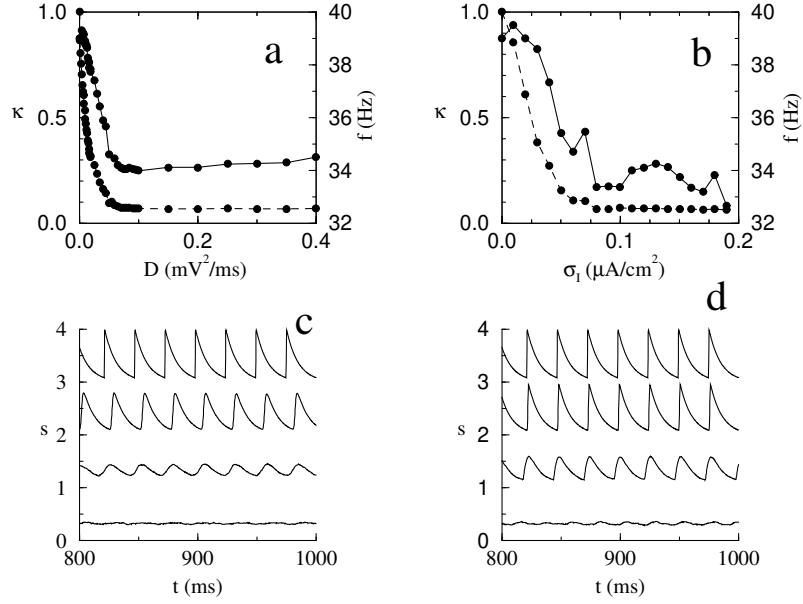
Figure 2. Noise and heterogeneity destroy strong synchronization. Coherence parameter κ (dashed curve, left-hand scale), and average network frequency f (continuous curve, right-hand scale) versus (*a*) noise strength D (with $\sigma_I = 0$) and (*b*) current heterogeneity σ_I (with $D = 0$). After a transient of 1 s, (*a*) time averages were computed over 3 s, and (*b*) 2 s. In (*b*) each point represents the results of one independent value of the current heterogeneity. In (*c*), (*d*) we plot the synaptic drive $s(t)$, (*c*) for $\sigma_I = 0$ with $D = 0, 0.01, 0.04$, and 0.09 from top to bottom; whereas in (*d*) $D = 0$ with $\sigma_I = 0, 0.01, 0.04, 0.09$ from top to bottom. The curves are offset by multiples of $\Delta s = 1$. We used the standard set of parameters described in the methods section.

4–5), and there is no dispersion in the cross correlations, only a relative phase. Even in the asynchronous state the autocorrelation function g_{X_i} for a single neuron is sharp, i.e. the neuron fires regularly with a fixed frequency (figures 3I(*c*)1 and (*c*)8). The population average of g_{X_i}, however, is disordered (figure 3I(*c*)7), since each of the neurons has a different firing rate. In the SN neurons case there is already dispersion due to the noise-induced jitter in the spike time, in the autocorrelation figure 3II(*a*)1, and in the cross correlations (figures 3II(*a*)2–5). The dispersion increases gradually with D. The difference between the CH and SN cases is also evident in the distribution of κ values for each pair in the network (figure 4, WB figure 8E). For SN there is a well defined peak, with the average shifting to lower values as D increases, (figures 4(*a*)–(*c*)), whereas for CH there is a broad distribution for small σ_I (figure 4(*d*)), a peak at low values of κ combined with a broad distribution for moderate values of σ_I (figure 4(*e*)). For higher values of σ_I the network is in an asynchronous regime, and only the peak for low κ values is present (figure 4(*f*)). We have compared the ISIH for a network neuron with the ISIH of an isolated neuron (not shown), and also the values of τ_{ISI} and σ_{ISI} (figures 5(*a*) and (*b*)). The CV of the network neuron is higher than the CV of an isolated neuron which in turn is higher than the CV of an isolated neuron with autosynaptic feedback. The inhibitory coupling in the network increases the effect of the noise compared with uncoupled neurons: the jitter in the spike times reduces the phasic component of $s(t)$ (figure 2(*c*)). This effect does not take place in a neuron with autosynaptic feedback: the size of the phasic component does not decrease with D, only the timing deteriorates.
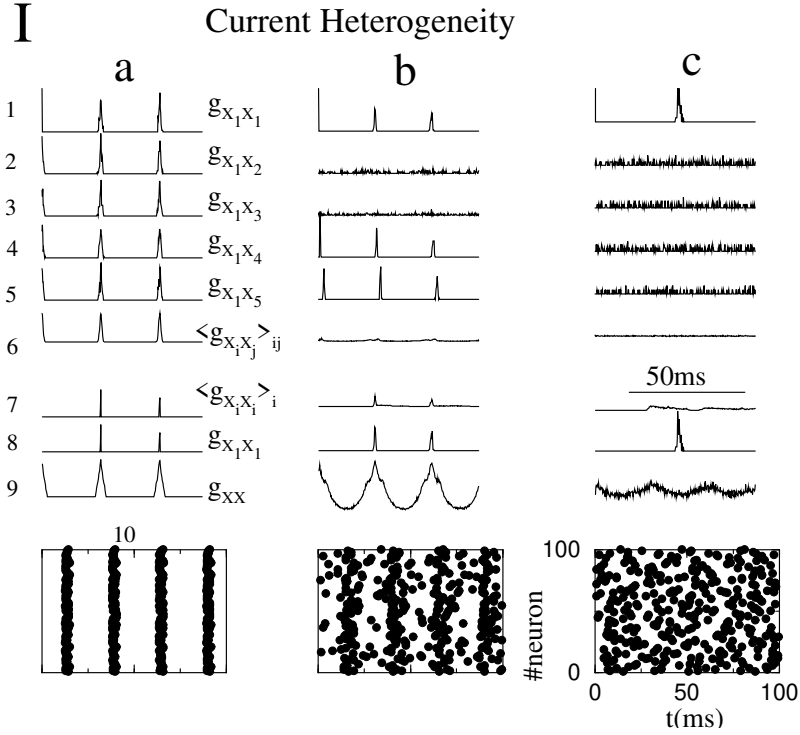
Figure 3. Noise and heterogeneity abolish strong synchronization in different ways: cross correlations. (I) Loss of synchrony due to current heterogeneities: (*a*) $\sigma_I = 0.02$, (*b*) 0.07, (*c*) 0.08, respectively. (II) Loss of synchrony due to synaptic noise: $D = 0.01$ (*a*), 0.04 (*b*), 0.09 (*c*), respectively. In 1 and 8 we plot the autocorrelation of X_1 (spike train of neuron 1); in 2–5 we plot the cross correlation of X_1 with $X_2, \ldots, X_5$, respectively; in 6 we show the cross correlations between X_i and X_j, averaged over all pairs i, j; in 7 we plot the autocorrelation of X_i, averaged over all neurons, and in 9 the auto correlation of the total spiking rate X; in 10 we show the rastergrams of the network, i.e. neuron number versus spiking time. The timescale bar, shown in I(*c*)7, applies to curves 1–9, (*a*)–(*c*) in I and II. The *y*-axis is in arbitrary units, and the same scale is used for the curves in 1–6, and 7–9, except for the curves II(*a*) 7,8 and II(*b*) 7,8, which are rescaled by a factor of 10. After a transient of 1 s, the time averages are computed over 2 s (I), and 3 s (II). We used the standard set of parameters described in the methods section.

3.2. Effect of synaptic coupling strength on robustness of strong synchronization

We have also studied the effect of varying the synaptic coupling strength g_{syn}. For large enough D the network will be asynchronous. We find that the network frequency in that case decreases with increasing values of g_{syn} (figure 6). For an asynchronous network the synaptic drive has a constant tonic hyperpolarizing conductance, decreasing the firing rate. The stronger the coupling the larger the decrease. The synchronization measured by the parameter κ displays a different behaviour. In figure 6(*c*) we plot the κ versus g_{syn} curve for one specific value $D = 0.02$. We have chosen I for each g_{syn} such that the firing rate is approximately 39 Hz, these current values are listed in the caption. It is interesting to note that in this case stronger coupling does not necessarily mean a higher value of κ. The coherence κ has a local maximum for $g_{\text{syn}} = 0.1$, for higher values of g_{syn}, κ decreases (see WB figure 12B). For $g_{\text{syn}} > 0.3$, κ starts increasing again. We have studied the underlying dynamics of this non-monotonous behaviour. In figures 7(*c*) and (*d*) we plot the ISIH for different values of g_{syn}. For $g_{\text{syn}} \geqslant 0.2$
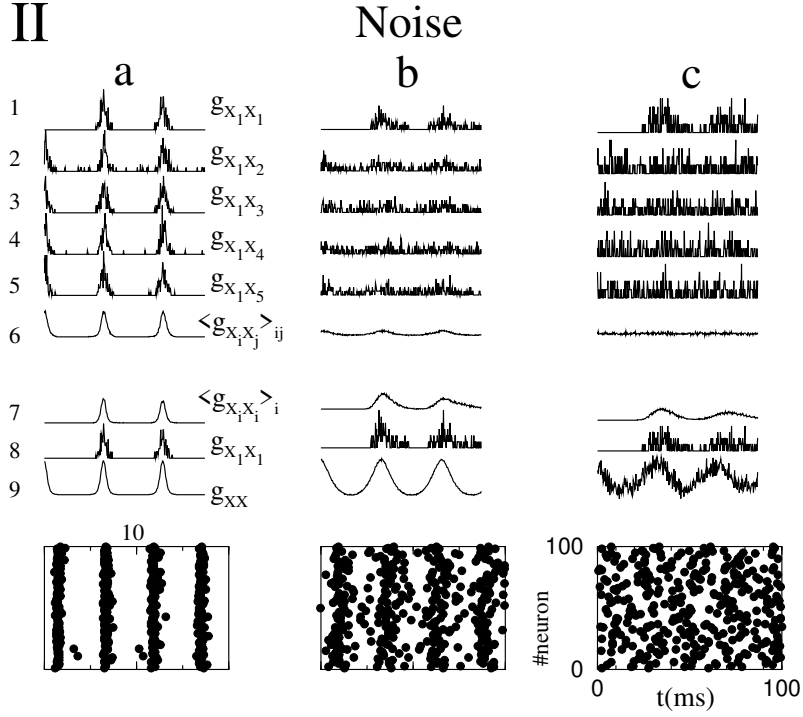
Figure 3. (Continued)

one finds more than one peak. In the rastergrams (figures 7(*a*) and (*b*)), one can see that the dynamics corresponds to a population that has a well defined frequency, but individual neurons sometimes miss, or skip, a period. Despite this small asynchrony when the neuron fires, it does so in synchrony with the others. As a consequence the rastergrams look much more ordered compared with the one for $g_{syn} = 0.1$ at the same noise strength $D = 0.002$.

3.3. Larger g_{syn} leads to robust stochastic weak synchronization

In this section we discuss the robust 40 Hz rhythms found for higher g_{syn} values. We have doubled the synaptic decay constant to $\tau_{syn} = 20$. Here we will evaluate the modified CV_W (equation (10)) and κ_W (equation (11)), characterizing the weak synchronization, as mentioned in the methods section.

In figure 8 we vary g_{syn} from 0.05 to 2.5 with a spacing of 0.05. The neuron number is kept equal to $N = 100$, and we use $I = 2.0$, and $\sigma_I = 0$. For $D = 0.0$ and $\sigma_I = 0$ the network is in a strongly synchronized state, with the network frequency f_n the same as the single-neuron firing rate f. The frequency is exactly the same as the one for a single neuron with autosynaptic feedback, as one would expect. This coherent state can be arrived at from many different random initial conditions.

For weak noise, $D = 0.008$, the network stays in a strongly synchronized state for $g_{syn} < 0.25$. For higher g_{syn} skipping starts to occur, the fractional cluster size decreases from values close to one to values below one-half at $g_{syn} = 1.2$. At that point the network
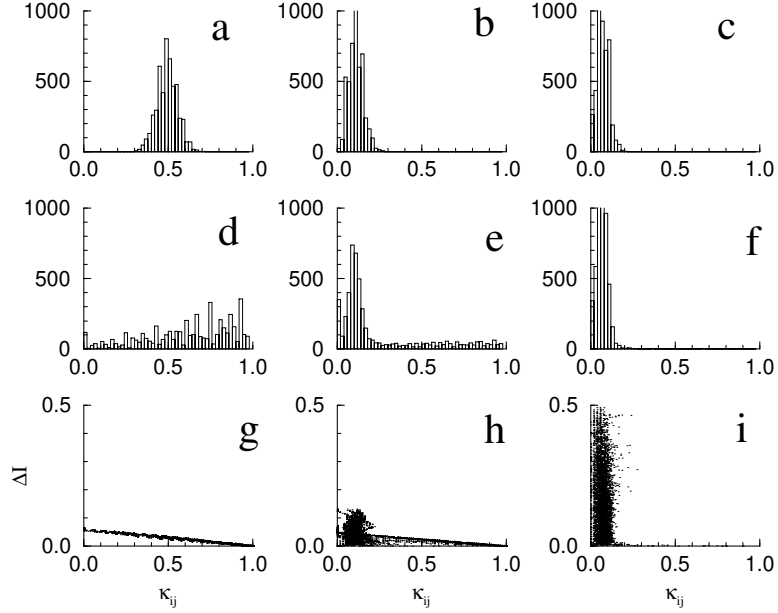
Figure 4. Noise and heterogeneity abolish strong synchronization in different ways: coincidence variables κ_{ij}. (a)–(f) distribution of κ values for individual pairs (i, j), (g)–(i) difference in driving current $\Delta I = |I_i - I_j|$ versus $\kappa_{i,j}$. In (a)–(c) $\sigma_I = 0$ and (a) $D = 0.01$, (b) 0.04, (c) 0.09. Whereas in (d)–(i) $D = 0$ and (d), (g) $\sigma_I = 0.02$, (e), (h) 0.04, and (f), (i) 0.15. A transient of 500 ms was discarded before averaging over 2000 ms. We used the standard set of parameters described in the methods section.
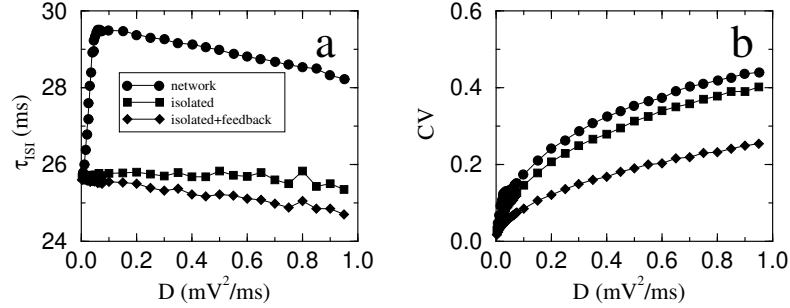

Figure 5. Inhibitory coupling increases the spike-time jitter in individual neurons. (a) Average interspike interval τ_{ISI}, and (b) coefficient of variation (CV), plotted versus noise strength D. We consider three different cases, averages over all neurons in the network (circles), isolated neuron with autosynaptic feedback (diamonds), isolated neuron without feedback (squares). For all curves $I = 1.0$ except for the single neuron without feedback, there $I = 0.61$. The averaging times are 10 s (network), and 200 s (isolated neuron).

is in a real (albeit stochastic) cluster state, on average the neuron only fires once every two cycles. We will refer to all states for which certain active neurons do not fire at each cycle as a SWS network. The network frequency, f_n, and the single-neuron firing rate, f, both decrease with increasing g_{syn}. When the network settles in the SWS state f starts to differ considerably from its value at the $D = 0$ state. The strength of synchronization increases with
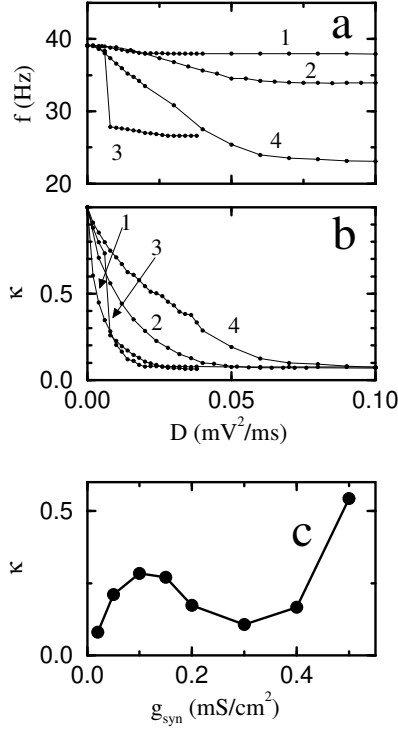
Figure 6. Coincidence κ at constant network frequency varies non-monotonously with coupling. (*a*) Network frequency, f, and (*b*) synchronization parameter, κ, plotted versus noise strength D, for different values of the synaptic coupling and applied current $(g_{\mathrm{syn}}, I) = (0.02, 0.6955), (0.1, 1.0), (0.3, 1.625)$, and $(0.5, 2.15)$, labelled by (1)–(4), respectively. The value of the applied current is chosen such that the neuron network will fire at $f \approx 39.05$ Hz at $D = 0$. In (*c*) we plot κ versus g_{syn} for $D = 0.02$ at the aforementioned current values. Time averages are computed over 10 s after a transient of 1 s.

g_{syn}, that is, CV_W decreases and κ_W increases. For values $g_{\mathrm{syn}} > 2.0$, CV_W and κ_W slowly saturate.

For stronger noise, say $D = 0.04$ and $D = 0.20$, the network is asynchronous for low values of g_{syn}. We have therefore excluded these points based on the criteria discussed in the methods section. The network frequency starts out at a higher value, and the neuronal firing rate at a lower rate compared with the $D = 0.008$ case. The strength of synchronization, κ_W and CV_W, is reduced compared with the one for $D = 0.008$, but still increases with g_{syn}. Note that all the neurons in the network still have a nonzero firing rate. We illustrate in figure 9, using rastergrams and the firing rate, how increasing g_{syn} for $D = 0.2$ drives the network from an asynchronous to a synchronized cluster state. It is thus possible to obtain weakly synchronized oscillations in a network consisting of 100 neurons in the frequency range between 20 and 40 Hz.

We find that noise is necessary to obtain SWS (figure 10). We have studied SWS in the presence of weak current heterogeneities, say for $\sigma_I = 0.02$. Without noise ($D = 0$) the network is in an strongly synchronized state, and κ displays a maximum as a function of g_{syn} (WB figure 12B). One also clearly notices the effect of suppression [21]: for larger g_{syn} the inhibition of faster spiking neurons stops the firing of neurons driven by a smaller current. As a result the total number N_s of active neurons gradually drops (figure 10(*f*)). For a small amount of noise, $D = 0.008$, the situation changes dramatically. A SWS state is obtained, and all neurons remain active ($N_s/N = 1$), while κ saturates for $g_{\mathrm{syn}} > 0.5$, and the value of κ for $g_{\mathrm{syn}} > 0.8$ is even higher than without noise. Thus noise may actually improve the coincidence. Of course noise does increase the width, CV_W, of the peaks in the instantaneous firing rate. The single neuron firing rate decreases significantly compared with that for $D = 0$, whereas the network frequency is only weakly affected.
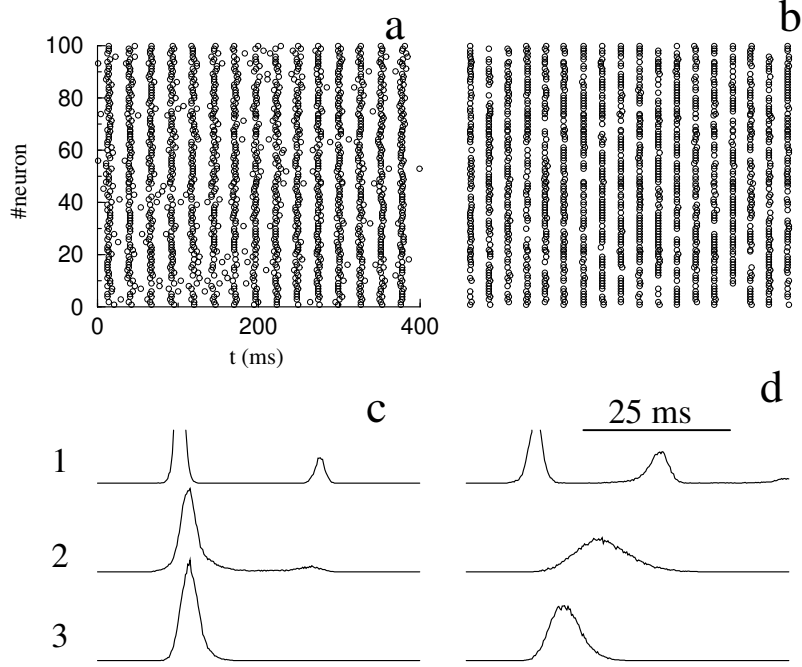
Figure 7. Stronger synaptic coupling leads to skipping of cycles. Rastergrams comparison, (*a*) $g_{syn} = 0.1$, $I = 1.0$, and (*b*) $g_{syn} = 0.5$, $I = 2.15$, with noise strength $D = 0.002$. We also compare the ISIHs for different values of the synaptic coupling $g_{syn} = 0.5$ (1), 0.2 (2), and 0.05 (3), and for different values of the noise strength D equal to (*c*) 0.014, (*d*) 0.034. The values of the applied currents are $I = 2.15$, 1.331, and 0.8145 for (1), (2), and (3), respectively. Timescale bar is shown in (*d*)1, the *y*-scale is arbitrary but the same for all curves in (*c*), (*d*). For clarity the top of (*c*)1 and (*d*)1 are cut off. An initial transient of 10 s in (*a*) and (*b*) was discarded. After a transient of 1 s, time averages were taken over 10 s (*c*), (*d*).

We have performed numerical simulations for system sizes $N = 10, 20, 50, 100, 200$, and 1000 (figure 11). We have used the following parameters values: $I = 5.0$, $D = 0.2$, $g_{syn} = 1$, $\tau_{syn} = 20$, and $\sigma_I = 0.1$. The network frequency increases with system size, whereas the firing rate stays approximately constant with a dip around $N = 50$. The measures for coherence, κ_W and CV_W, are also only weakly dependent on the system size.

The cycle-to-cycle fluctuations in cluster size vary approximately as $\sqrt{N}$ (figure 11(*g*)). The strength of the inhibition is determined by the number of neurons that fired in the previous cluster, and in turn it determines at what time the first neurons become disinhibited. One therefore expects cluster size fluctuations and cycle length fluctuations to be intimately related. Indeed, the standard deviation of cycle length varies as $1/\sqrt{N}$ with N the number of neurons (figure 11(*h*)). This means that larger networks are better at generating a precise cycle length, whereas size does not matter as much for the coincidence of spikes measured by κ_W and CV_W.

In each simulation we randomly draw a set of driving currents I_j for each neuron j from a uniform probability distribution. The results one obtains may critically depend on the particular realization of driving currents. One expects that for larger systems this is less of a problem. The population distribution of I is more likely to approach the original ensemble distribution of currents for a given neuron. Here we have studied the range of values for the measured quantities (f_n, f, and so on) for ten different realizations. We find that for most quantities (for
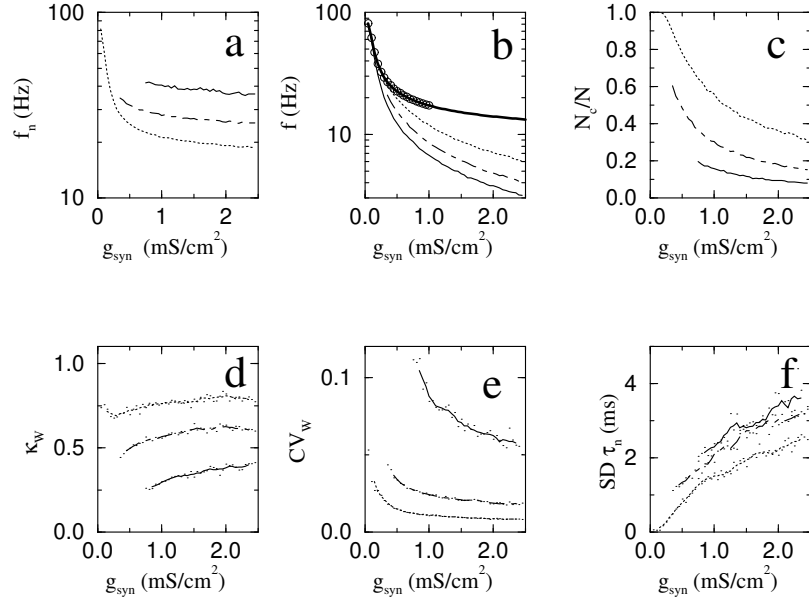
Figure 8. Properties of SWS as function of the synaptic coupling strength. We plot (*a*) network frequency f_n, (*b*) single-neuron firing rate f, (*c*) cluster size N_c normalized by system size $N = 100$, (*d*) κ_W, (*e*) coefficient of variation CV_W of ISI, and (*f*) standard deviation of the network period τ_n versus synaptic strength g_{syn}, for different values of $D = 0.008$ (dotted curves), $D = 0.04$ (dot-dashed curves) and $D = 0.2$ (solid curves). g_{syn} is varied from 0.05 to 2.5 in increments of 0.05. For $D = 0.04$ ($D = 0.2$) the first 6 (14) points have been removed according to the criterium given in the methods section. In (*b*) we have added the firing rate of a single neuron with autosynaptic feedback (thick solid curve), and the network for $D = 0$ (open circles). Other parameters are $\sigma_I = 0$, $I = 2.0$, $\tau_{syn} = 20$. A 500 ms transient is discarded, and averages are taken over 2000 ms. To smooth (*d*)–(*f*) we have performed running averages over five points, the original points are denoted by dots.

these parameter values) the range of values decreases with N, and for $N \geqslant 500$ one realization will give a result close to the expectation value.

We now vary σ_I and D for the following fixed parameter set $N = 1000$, $g_{syn} = 2$, $\tau_{syn} = 20$, and $I = 3.5$ (figures 12, 13). For $D = 0$ and $\sigma_I = 0$ the network is strongly synchronized at 20 Hz. The instantaneous firing rate consists of a sequence of regularly spaced delta functions (figure 12(*e*)), the ISIH has a single delta peak at 50 ms (figure 12(*b*)), and all neurons spike at the same frequency (figure 12(*a*)). Increasing D increases the network frequency, but decreases the single-neuron firing rate (figure 13). The population activity is still periodic (figure 12(*f*)), but the peaks have a finite width (as well as the ISIH), and the ISIH becomes multimodal. This process continues with the ISIH spreading out more and more, with the CV_W increasing, and κ_W decreasing.

As mentioned before we need some noise to generate an SWS state. Here we use $D = 0.2$, while at the same time varying σ_I. For finite σ_I there is still a coherent population activity (figure 12(*g*)), despite the fact that neurons have different firing rates (figure 12(*c*)). Increasing σ_I will reduce coherence, κ_W decreases and CV_W increases. At the same time both f_n and f increase (figure 13(*d*)). This is different from the effect of increasing D. Higher σ_I leads to suppression, with fast spiking neurons preventing slower ones from firing, and as a result part of the inhibition disappears, while further increasing the firing rate and its average (calculated
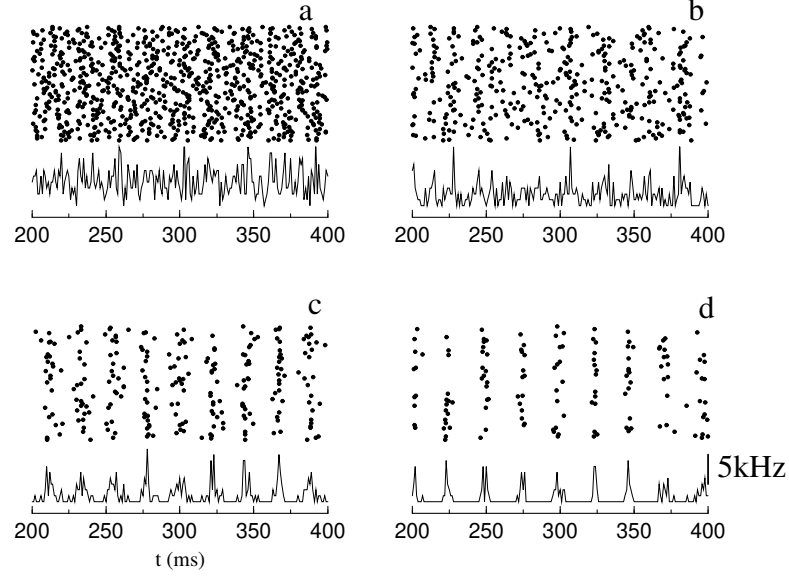
Figure 9. Increasing synaptic coupling leads to synchronized network oscillations. We plot in each panel (top) rastergrams and (bottom) instantaneous firing rates, with bin size 1 ms. The data represent four points on the $D = 0.2$ curves in figure 8 at (*a*) $g_{syn} = 0.15$, (*b*) 0.3, (*c*) 0.5, (*d*) 1.0. The scale bar in (*d*) corresponds to five spikes in a 1 ms bin.
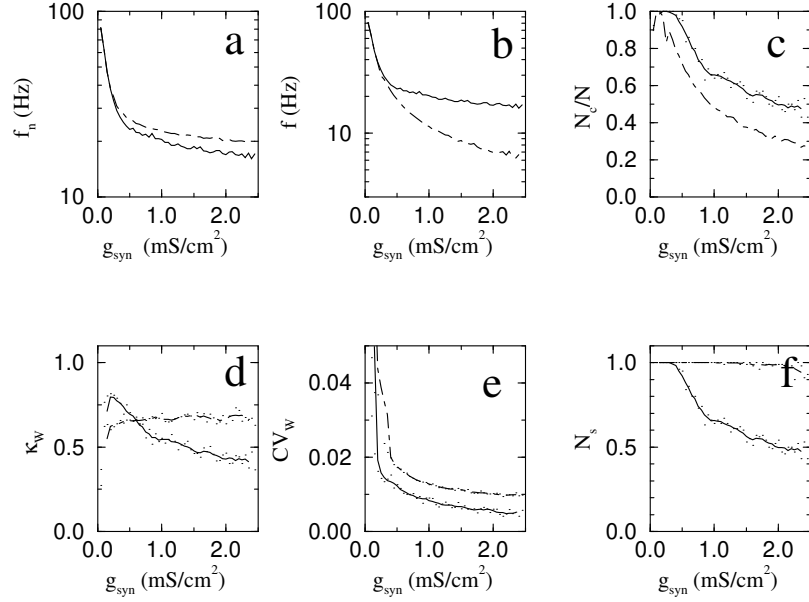

Figure 10. Noise can prevent suppression and can increase coincidence κ_W. We plot (*a*)–(*e*) as in figure 8, (*f*) number N_s of active neurons for different values of $D = 0.0$ (solid curves), $D = 0.008$ (dot-dashed curves). Other parameters are $\sigma_I = 0.02$, $I = 2.0$, $\tau_{syn} = 20$. The smoothed (*c*)–(*f*) plots were obtained as in figure 8.
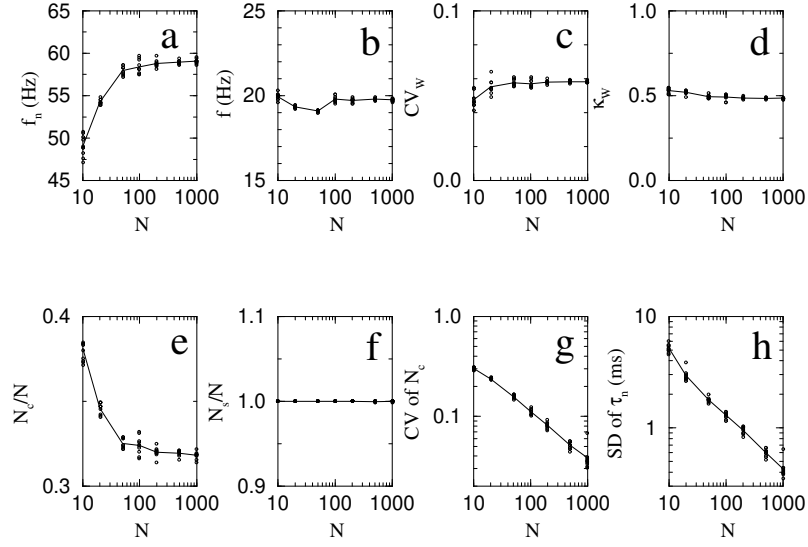
Figure 11. Most network properties saturate for $N > 100$. We plot (*a*) network frequency f_n, (*b*) single-neuron firing rate f, (*c*) coefficient of variation CV_W of ISI, (*d*) κ_W, (*e*) cluster size N_c normalized by system size N, (*f*) number of active neurons N_s normalized by N, (*g*) coefficient of variation of N_c, (*h*) standard deviation of the network period τ_n versus system size N ($N = 10, 20,$ 50, 100, 200, 500, 1000). We show results for ten different realizations of the current distribution (open circles), and their average (solid curves). Other parameters are $\sigma_I = 0.10$, $D = 0.2$, $I = 5.0$, $g_{\rm syn} = 1.0$, and $\tau_{\rm syn} = 20$. A 500 ms transient is discarded, and averages are over at least 2000 ms.

from the active neurons). (Note that the suppression here is different from that at $D = 0$, the fast spiking neurons still produce a periodic population oscillation.) On the other hand, noise increases the tonic inhibition for each neuron, and thus leads to a reduced firing rate. In addition, the progression of the asynchronous state is different. The first peak in the ISIH becomes broader, and the higher order ones have a reduced prominence (figure 12(*d*)). For increasing D the peaks just wash out.

3.4. A single neuron driven by a simulated network input

A neuron in a network of neurons is driven by other neurons by a spike train of IPSPs (with unitary conductance $g_{\rm syn}/N$). The statistics of the spike trains are given by the instantaneous firing rate $\hat{X}(t)$, which in turn can be characterized by a period τ_n, cluster size N_c, and jitter σ_c (see the methods section and figure 1). We have investigated the dynamics of a single neuron driven by a simulated network input (figure 14). We generate spike trains as a Poisson process from a realistic $\hat{X}(t)$, with parameters $\tau_n = 25$, $N = 100$, $N_c = 62.5$, $\sigma_c = 0.5$ ($CV_W = 0.02$), and inject these into the neuron. The input corresponds to that of a weakly synchronized network, $N_c < N$. However, since the inputs are independent, it may also be interpreted as a strongly synchronized network with a synaptic strength $g_{\rm syn}N_c/N$ and consisting of N_c neurons. The neuron is weakly synchronized to the network's input when its average phase ϕ is close to the phase of the input, $\frac{1}{2}$, and the output jitter σ_ϕ is not much larger than CV_W. (Note that σ_ϕ averaged over all network neurons would be equal to CV_W.) Strong synchronization requires that all neurons also fire with the same period, that is $f = 40$ Hz. In figure 14 we compare the weak coupling case, $g_{\rm syn} = 0.1$, to the strong coupling case,
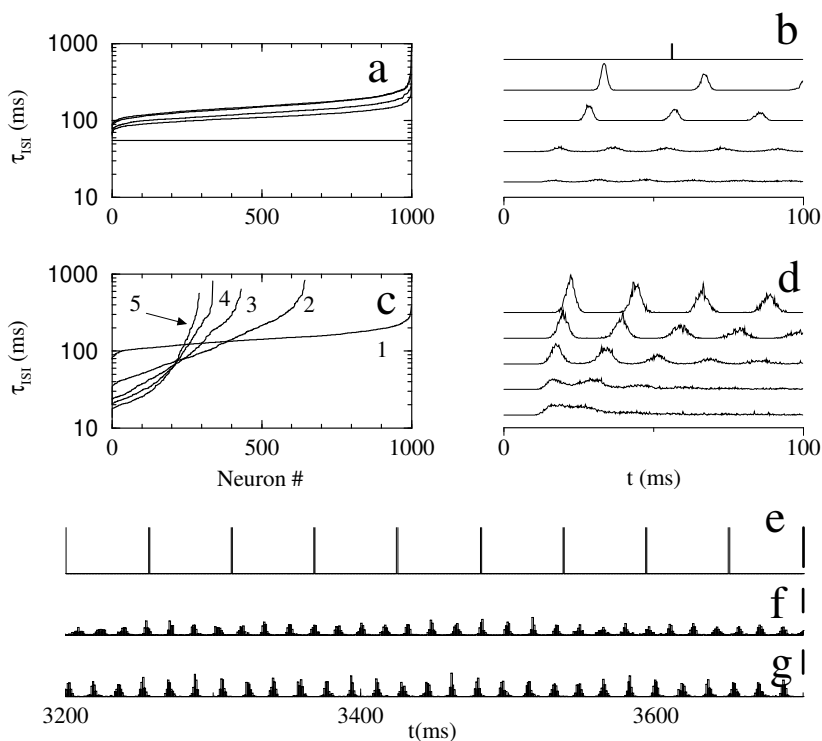
Figure 12. Synchronized network oscillations can exist despite large variations in the individual spiking rates. We plot in (*a*), (*c*) the interspike intervals (ISI) of the network neurons sorted from the lowest to highest value, and (*b*), (*d*) the ISIHs. In (*a*), (*c*) we used different values of the noise strength, from top to bottom $D = 0.0, 0.04, 0.08, 0.36$, and 0.56, with $\sigma_I = 0$. In (*c*), (*d*) from top to bottom $\sigma_I = 0$ (1), 0.173 (2), 0.346 (3), 0.520 (4), and 0.693 (5), with $D = 0.2$. After a transient of 500 ms, the time average is computed over 2 s. We plot the instantaneous firing rate as a function of time for (*e*) $D = 0, \sigma_I = 0$, (*f*) $D = 0.56, \sigma_I = 0$, and (*g*) $D = 0.2, \sigma_I = 0.35$. The scale bars are (*e*) 500 imp s^{-1}, (*f*), (*g*) 50 imp s^{-1}. We used $I = 3.5, \tau_{\text{syn}} = 20, N = 1000$, and $g_{\text{syn}} = 2.0$.

$g_{\text{syn}} = 1.0$. In both cases the firing rate of the neuron increases with increasing current drive (figures 14(*c*) and (*f*)). A prominent feature here is the presence of an entrainment step. On an entrainment step the firing rate is constant for a range of current values, and equal to a fraction of the driving frequency, $\frac{n}{m} f_{\text{drive}}$ (the neuron fires n action potentials during m cycles of the external drive). In this case $n = m = 1$. For weak coupling the jitter σ_ϕ is only small on the entrainment step itself (figure 14(*b*)). However, on the step, ϕ varies with the value of the current drive (figure 14(*a*)). The phase ϕ will only be close to $\frac{1}{2}$ for a small current range. This generic feature of entrainment steps explains why strong synchronization is not robust against current heterogeneity. We have also studied the effect of a noise current with $D = 0.04$. The jitter increases dramatically, $\sigma_\phi > 0.2$, even for current values on the $D = 0$ entrainment step. In other words, strong synchronization is also not very robust against noise.

We now discuss the strong coupling case. For current values below the entrainment step there is a large current range where ϕ is close to $\frac{1}{2}$, and $\sigma_\phi < 0.05$. Here one would obtain weak synchronization in the network case. This state is thus more robust against current heterogeneity. We note that it is hard to distinguish the $D = 0$ from the $D = 0.04$ curves (figures 14(*d*)–(*f*)). The dynamics here is therefore also more robust against noise.
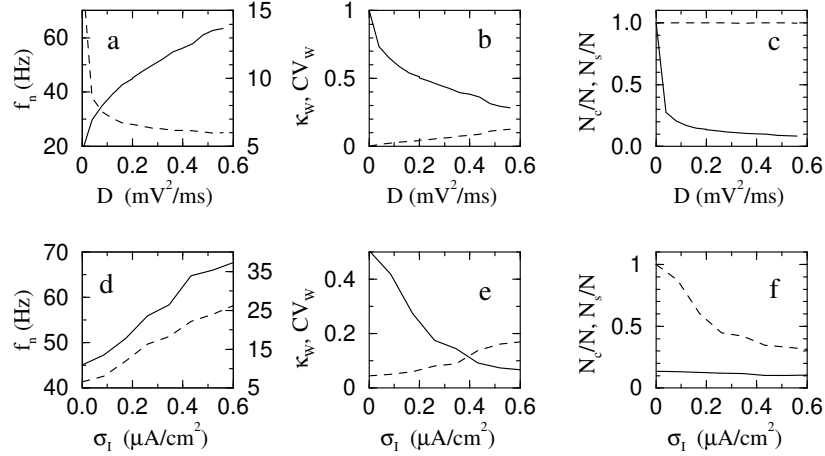
Figure 13. Variation of SWS properties as a function of noise and as a function of heterogeneity. We plot in (*a*), (*d*) the network frequency f_n (solid curve, left-hand scale) and single neuron firing rate f (dashed curve, right-hand scale); (*b*), (*e*) coherence κ_W (solid curve) and the CV_W (dashed curve); (*c*), (*f*) cluster size N_c and number of active neurons N_s divided by N; as function of (*a*)–(*c*) noise variance D, and (*d*)–(*f*) current heterogeneity σ_I. We used the following parameters $I = 3.5$, $\tau_{\text{syn}} = 20$, $g_{\text{syn}} = 0$, and $N = 1000$, for (*a*)–(*c*) with $\sigma_I = 0$, and for (*d*)–(*f*) the same parameters with $D = 0.2$.

4. Discussion

Previous authors have recognized that strong synchronization is only moderately robust against neuronal heterogeneity [20, 21]. We have previously shown that the same holds if we include synaptic noise [22]. The basic premise of synchronization by mutual inhibition is clear, for the network consists of intrinsically periodically spiking neurons. Their output produces a periodic synaptic drive, which in turn is fed back into the network. Inhibition thus allows a phase lock at zero relative phase with this drive. Heterogeneity and noise reduces the phasic, and increases the tonic part of the synaptic drive, leading to a reduction in synchronization, and eventually leading to an asynchronous state (figures 2(*c*) and (*d*)). The synchronization behaviour of networks of physiological realistic neurons, however, is by no means fully understood. In this work we showed that the loss of synchronization proceeds via different mechanisms in the presence of synaptic noise compared with the presence of current heterogeneity. This is evident from the cross correlations shown in figures 3 and 4. We also found that the noise-induced precision loss in the uncoupled neuron is exacerbated by the inhibitory coupling. All of these could seem obvious based on previous work on heterogeneity [20, 21]. However, its consequences for real-life biological networks had not been fully appreciated before. Our results, combined with previous results, show that there is a problem with strong synchronization by mutual inhibition, since it is unlikely to occur in *in vitro* or *in vivo* systems. (There are exceptions, such as for example the pacemaker nucleus in electric fish [49], where the neurons are coupled via gap junctions.) The aim of this paper was to treat the problem of how one can obtain robust synchronization in the presence of synaptic noise and neuronal heterogeneity. Our results are twofold. First, methods to increase the robustness of strong synchronization have been ineffective. Second, we showed that robust SWS can be obtained for biophysically realistic parameter values. SWS is consistent with previous experimental data. In what follows we discuss these two results in more detail.
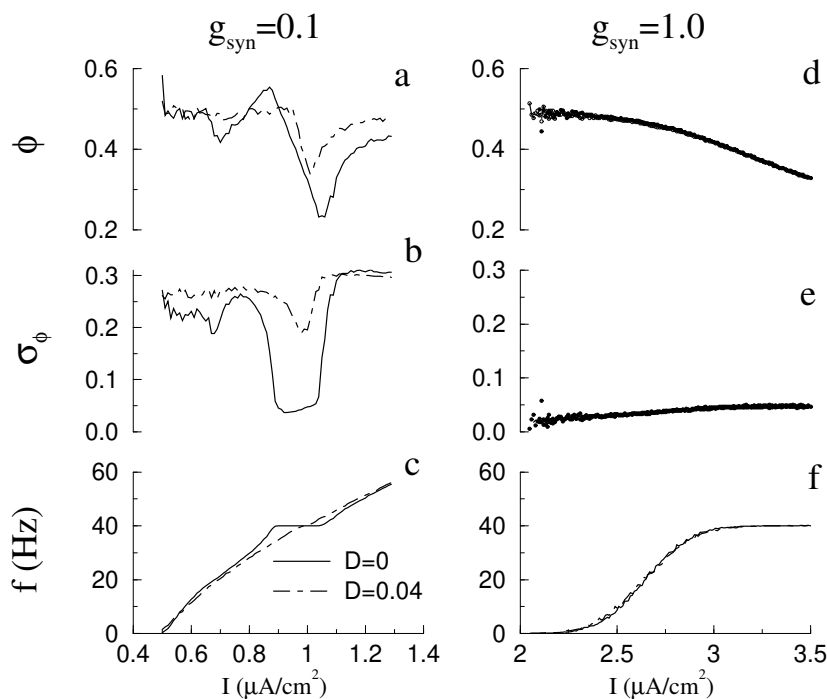
Figure 14. Response of single neuron to simulated network input. We plot in (*a*), (*d*) the average phase ϕ, (*b*), (*e*) the phase jitter σ_ϕ, and (*c*), (*f*) the firing rate f. The coupling strength in (*a*)–(*c*) is $g_{\mathrm{syn}} = 0.1$, and in (*d*)–(*f*) 1.0. The noise strengths are $D = 0$ (solid curves), and $D = 0.04$ (dot-dashed curves). In (*d*), (*e*) the lines represent running averages over five points, the actual data are denoted by dots. The network input consists of $N = 100$ neurons of which $N_c = 62.5$ fire each cycle, $\tau_n = 25$, $\sigma_c = 0.5$ (i.e. $CV_W = 0.02$), and the unitary conductance is $g_{\mathrm{syn}}/100$ (see the methods section for details). The input phase is defined as $\phi = \frac{1}{2}$. A transient of 500 ms was discarded, and averages were calculated over 5×10^4 ms.

From the results stated above, we believe that strong synchronization is not robust enough. To make sure that we do not prematurely discard strong synchronization by mutual inhibition we made an effort to increase its robustness. In this paper we tried two simple methods to increase robustness of strong synchronization. One was to increase the synaptic coupling g_{syn}, since inhibition is responsible for synchronization. It is then quite natural to expect that increasing the strength of inhibition increases robustness. The fact that this does not happen is surprising. For current heterogeneity this is in part due to suppression [20, 21]. We have also studied this effect for synaptic noise in more detail. We found that neurons skip periods for higher values of g_{syn} (see figure 7). In other words, the strongly synchronized state becomes unstable, and a weakly synchronized state emerges. This weakly synchronized state looked more coherent (figures 7(*a*) and (*b*)), and it provided the impetus for our further studies of the robustness of the SWS states.

Recent experimental work shows that the CV of neurons on an entrainment step is reduced compared with the CV outside the step [50]. A clear physiological correlate in hippocampus of this drive, however, is lacking at present time. Since we tried to reject our conjecture, this lack of physiological realism is not a problem. We did find a moderate increase in robustness with a periodic drive, that is not as effective as one would have intuited, however (Tiesinga and José,

unpublished observations). In fact the inhibitory connections reduce the increase in robustness compared with the increase in the single uncoupled neuron. If we add a subthreshold periodic drive with noise to a quiescent neuron we obtain weak synchronization. This is known as stochastic resonance in excitable systems [51]. To summarize: our attempts to significantly increase robustness of strong synchronization failed. Instead we found weak synchronization, which turned out to be easier to find in parameter space than strong synchronization.

If one accepts the fact, however, that strong synchronization is not robust against noise and heterogeneity, and that periodic population oscillations are found in experiments, then one has to carefully consider the possible relevance of weak synchronization. Weak synchronization as well as strong synchronization lead to a periodic population discharge, and specifically to an inhibitory synaptic drive indistinguishable from the one found in pyramidal neurons in [14]. Moreover, the clusters that form in stochastic weak synchronization bear a resemblance to the neuronal assemblies found in some experiments [52], and that are thought to play a role in putative binding [53]. The question then is: is SWS more robust, and can it be found for the gamma-frequency range for biophysically realistic parameters? What is needed is a higher total synaptic conductance, and noise. The necessary amount of noise is very small, i.e. $D > 0.004$ is sufficient. The noise prevents the occurrence of suppression (figure 10). In suppression the faster neurons prevent the slower ones from firing. This reduces the inhibition of the faster ones, and allows them to fire at different frequencies and at a random relative phases. Suppression is thus detrimental to synchronization. Noise-induced jitter helps suppressed neurons to escape. (Note: for strong heterogeneities suppression can also occur at non-zero noise, see figure 13 and the corresponding text. However, there is still a periodic discharge in that case.) A higher total synaptic conductance is necessary for two reasons. The inhibition generated by a cluster, i.e. only part of the network, should be strong enough to prevent the other neurons from firing out of sync. In addition this effective inhibition should be stronger than that necessary one for the strong synchronization we obtained here. This becomes clear when considering a single neuron driven by a simulated network input. For strong synchronization one can choose a current value on the entrainment step (see figure 14). An entrainment step exists for any value of g_{syn}. Of course, the current range for which the step occurs, varies. However, weak synchronization occurs below the entrainment step. For weak coupling, $g_{\mathrm{syn}} = 0.1$, the output jitter σ_ϕ is too high to allow for a synchronized state. The jitter will only be low enough for significantly stronger coupling, e.g. $g_{\mathrm{syn}} = 1.0$ (figure 14(*e*)).

We obtained SWS for different system sizes (we studied networks from 10 to 1000 neurons). The coincidence properties (κ_W, and CV_W) did not vary much with size. The temporal precision of the population oscillation, however, increases approximately as $1/\sqrt{N}$ (figure 11(*h*)). Large networks can thus produce precise pacemaker rhythms. In addition, the statistical quantities in a small networks show more variation with different realizations of the current drive.

It is of considerable interest to understand why weak synchronization is so much more robust and prevalent compared with strong synchronization. In strong synchronization one requires an equal firing rate for each neuron, while weak synchronization requires only close coincident spikes. By definition, then, weak synchronization is easier to generate. Strong synchronization is only possible (depending on intrinsic properties) for a small difference in driving currents. There is a price to pay, for there will be a phase difference between the firings of each neuron. Pairs with a large phase difference are less stable against the influence of noise. Strong synchronization can thus only occur if all neurons have roughly the same intrinsic spiking frequency, or when there is a gap junction coupling between them. In section 3.3 we found network parameters for which coincidence could be maintained, despite highly variable and noisy firing rates of the neuronal populations. The allowable levels of σ_I and D for which

one still obtains SWS are much higher than the $\sigma_I < 0.10$ and $D < 0.10$ for which strong synchronization was obtained by Wang and Buzsáki [20].

Our work, and also a recent study [21], is to a large extent based on the recent contributions by Wang and Buzsáki [20]. It is therefore important to briefly reiterate, and spell out how our work extends the work of Wang and Buzsáki, and how it differs from the work of White *et al* [21]. Here we have included the effect of synaptic noise, that was not considered by Wang and Buzsáki. We have shown that for the purposes of our modelling work a Gaussian white noise current can adequately reproduce experimental ranges of CV [47]. We found that biophysically realistic amounts of noise do affect the synchronization we have studied. As we discussed above, the noise effects are also different from those of current heterogeneity. Another important difference is that previous works [20,21] only studied strong synchronization. Here we have proposed that stochastic weak synchronization underlies the synchronized population oscillations in the hippocampus. For this reason our robust 40 Hz population rhythms were obtained for different values of the coupling parameters g_{syn}, τ_{syn}, the driving current I, and the system size N, as compared with previous work [20]. In our computational work we actually needed a small amount of noise to be able to generate weak synchronization.

The synchronization properties of large networks may be of some mathematical interest. Our networks are small, and probably the behaviour can change quantitatively when increasing the network size significantly. However, in this paper we only addressed the question as to whether networks of physiologically realistic size and connectivity can robustly synchronize. Recent experimental work suggests that interneurons contact on the order of 60 other interneurons [54]. For this reason we only vary our network size between $N = 10$ and 1000.

In the introduction we mentioned recent *in vivo* work and the controversies on the functional relevance and role played by synchronization. Our work obviously does not contribute to the understanding of the function of synchronization. An important question is what kind of synchronization can be sustained in biophysically realistic networks. Traub and co-workers [12–15] looked for physiological correlates of the gamma rhythms using *in vitro* experiments and computational modelling. Their results show the crucial role of inhibition, and have provided much of the impetus for our work. The nervous system produces, for some unknown reason, periodic population activity using circuitry consisting of noisy and heterogeneous neurons. Our results establish that it is possible for inhibitory neurons to be the driving force for synchronization under these conditions. In future work we will investigate what role these interneurons play in generating gamma-oscillations in full networks consisting of inhibitory interneurons and excitatory pyramidal cells [55].

References

[1] Adrian E D 1950 The electrical activity of the mammalian olfactory bulb *Electroencephalogr. Clin. Neurophysiol.* **2** 377–88

[2] Softky W R and Koch C 1993 The highly irregular firing of cortical cells is inconsistent with temporal integration of random EPSPs *J. Neurosci.* **13** 334–50

[3] Gur M, Beylin A and Snodderly D M 1997 Response variability of neurons in primary visual cortex (V1) of alert monkeys *J. Neurosci.* **17** 2914–20

[4] Aertsen A and Arndt M 1993 Response synchronization in the visual cortex *Curr. Opin. Neurobiol.* **3** 586–94

[5] Rieke F, Warland D, de Ruyter van Steveninck R R and Bialek W 1997 *Spikes: Exploring the Neural Code* (Cambridge, MA: MIT Press)

[6] Softky W R 1995 Simple codes versus efficient codes *Curr. Opin. Neurobiol.* **5** 239–47

[7] Shadlen M N and Newsome W T 1994 Noise, neural codes, and cortical organization *Curr. Opin. Neurobiol.* **4** 569–79

[8] Shadlen M N and Newsome W 1995 Is there signal in the noise (comment)? *Curr. Opin. Neurobiol.* **5** 248–50

[9] Shadlen M N and Newsome W T 1998 The variable discharge of cortical neurons: implications for connectivity, computation, and information coding *J. Neurosci.* **18** 3870–96

[10] Stopfer M, Bhagavan S, Smith B H and Laurent G 1997 Impaired odor discrimination on desynchronization of odor-encoding neural assemblies *Nature* **390** 70–4

[11] Prut Y, Vaadia E, Bergman H, Haalman I, Slovin H and Abeles M 1998 Spatiotemporal structure of cortical activity: properties and behavioural relevance *J. Neurophysiol.* **79** 2857–74

[12] Traub R D, Whittington M A, Colling S B, Buzsaki G and Jeffreys J G R 1996 Analysis of gamma rhythms in the rat hippocampus *in vitro* and *in vivo J. Physiol.* **493** 471–84

[13] Whittington M A, Traub R D, Faulkner H J, Jefferys J G R and Chettiar K 1998 Morphine disrupts long-range synchrony of gamma oscillations in hippocampal slices *Proc. Natl Acad. Sci. USA* **95** 5807–11

[14] Whittington M A, Traub R D and Jeffreys J G R 1995 Synchronized oscillations in interneuron networks driven by metabotropic glutamate receptor activation *Nature* **373** 612–5

[15] Traub R D, Whittington M A, Stanford I M and Jeffreys J G R 1996 A mechanism for generation of long-range synchronous fast oscillations in the cortex *Nature* **383** 621–4

[16] Fisahn A, Pike F G, Buhl E H and Paulsen O 1998 Cholinergic induction of network oscillations at 40 Hz in the hippocampus *in vitro Nature* **394** 186–9

[17] Fellous J-M and Sejnowski T J 2000 Cholinergic induction of oscillations in the hippocampal slice in the slow (0.5–2 Hz), theta (5–12 Hz) and gamma (35–70 Hz) bands *Hippocampus* at press

[18] van Vreeswijk C, Abbott L F and Ermentrout G B 1994 When inhibition not excitation synchronizes neural firing *J. Comput. Neurosci.* **1** 313–22

[19] Wang X-J 1993 Ionic basis for intrinsic 40 Hz neuronal oscillations *Neuroreport* **5** 221–4

[20] Wang X J and Buzsáki G 1996 Gamma oscillation by synaptic inhibition in a hippocampal interneuronal network model *J. Neurosci.* **16** 6402–13

[21] White J A, Chow C C, Ritt J, Soto-Treviño C and Kopell N 1998 Synchronization and oscillatory dynamics in heterogeneous, mutually inhibited neurons *J. Comput. Neurosci.* **5** 5–16

[22] Tiesinga P H E, Rappel W-J and José J V 1998 Synchronization in networks of noisy interneurons *Computational Neuroscience* ed J Bower (New York: Plenum) pp 555–9

[23] Brunel N and Hakim V 1999 Fast global oscillations in networks of integrate-and-fire neurons with low firing rates *Neural Comput.* **11** 1621–71

[24] Amit D J and Brunel N 1997 Model of global spontaneous activity and local structured activity during delay periods in the cerebral cortex *Cereb. Cortex* **7** 237–52

[25] Tiesinga P H E and José J V 2000 Synchronous clusters in a noisy inhibitory neural network *J. Comput. Neurosci.* at press

[26] Golomb D and Rinzel J 1994 Clustering in globally coupled inhibitory neurons *Physica* D **72** 259–82

[27] Golomb D and Rinzel J 1993 Dynamics of globally coupled inhibitory neurons with heterogeneity *Phys. Rev.* E **48** 4810–4

[28] Golomb D and Rinzel J 1994 Synchronization properties of spindle oscillations in a thalamic reticular nucleus model *J. Neurophys.* **72** 1109–26

[29] Kopell N and LeMasson G 1994 Rhythmogenesis, amplitude modulation, and multiplexing in a cortical architecture *Proc. Natl Acad. Sci. USA* **91** 10 586–90

[30] Rall W 1995 Perspective on neuron model complexity *Handbook of Brain Theory and Neural Networks* ed M A Arbib (Cambridge, MA: MIT Press) pp 728–32

[31] Pinsky P F and Rinzel J 1994 Intrinsic and network rhythmogenesis in a reduced Traub model for CA3 neurons

J. Comput. Neurosci. **1** 39–60

[32] Mainen Z F and Sejnowski T J 1994 Influence of dendritic structure on firing pattern in model neocortical neurons *Nature* **383** 363–6

[33] Mainen Z F and Sejnowski T J 1998 Modelling active dendritic processes in pyramidal neurons *Methods in Neuronal Modelling* ed C Koch and I Segev (Cambridge, MA: MIT Press) pp 171–209

[34] Yuste R and Tank D W 1996 Dendritic integration in mammalian neurons, a century after Cajal *Neuron* **16** 701–16

[35] Koch C 1997 Computation and the single neuron *Nature* **385** 207–10

[36] Larkum M E, Zhu J J and Sakmann B 1999 A new cellular mechanism for coupling inputs arriving at different cortical papers *Nature* **398** 338–41

[37] Perkel D H, Mulloney B and Rudelli R W 1981 Quantitative methods for predicting neuronal behaviour *Neuroscience* **56** 823–7

[38] Wang X-J and Rinzel J 1993 Spindle rhythmicity in the reticularis thalami nucleus: synchronization among mutually inhibitory neurons *Neuroscience* **53** 899–904

[39] Buhl E H, Cobb S R, Halasy K and Somogyi P 1995 Properties of unitary IPSPs evoked by anatomically identified basket cells in the rat hippocampus *Eur. J. Neurosci.* **7** 1989–2004

[40] Greenside H S and Helfand E 1981 Numerical integration of stochastic differential equations *Bell Syst. Tech. J.* **60** 1927

[41] Press W H, Teukolsky S A, Vetterling W T and Flannery B P 1992 *Numerical Recipes* (Cambridge: Cambridge University Press)

[42] Lacaille J-C, Mueller A L, Kunkel D D and Schwartzkroin P A 1987 Local circuit interactions between oriens-alveus interneurons and CA1 pyramidal cells in hippocampal slices: electrophysiology and morphology *J. Neurosci.* **7** 1979–93

[43] Lacaille J-C and Williams S 1990 Membrane properties of interneurons in stratum oriens-alveus of the CA1 region of rat hippocampus *in vitro Neuroscience* **36** 349–59

[44] Morin F, Beaulieu and Lacaille J-C 1996 Membrane properties and synaptic currents evoked in CA1 interneuron subtypes in rat hippocampal slices *J. Neurophys.* **76** 1–16

[45] Johnston D and Wu M 1995 *Foundations of Cellular Neurophysiology* (Cambridge, MA: MIT Press)

[46] Calvin W H and Stevens C F 1967 Synaptic noise as a source of variability in the the interval between action potentials *Science* **155** 842–3

[47] Tiesinga P H E and José J V 1999 Spiking statistics in noisy hippocampal interneurons *Neurocomputing* **26–27** 299–304

[48] Rodieck R W, Kiang NY-S and Gerstein G L 1962 Some quantitative methods for the study of spontaneous activity of single neurons *Biophys. J.* **2** 351–68

[49] Moortgat K T, Keller C H, Bullock T H and Sejnowski T J 1998 Submicrosecond pacemaker precision is behaviourally modulated: the gymnotiform electromotor pathway *Proc. Natl Acad. Sci. USA* **95** 4684–9

[50] Hunter J D, Milton J G, Thomas P J and Cowan J D 1998 Resonance effect for neural spike time reliability *J. Neurophysiol.* **80** 1427–38

[51] Wiesenfeld K and Moss F 1995 Stochastic resonance and the benefits of noise: from ice ages to crayfish and SQUIDs *Nature* **373** 33–6

[52] MacLeod K and Laurent G 1996 Distinct mechanisms for synchronization and temporal patterning of odor-encoding neural assemblies *Science* **274** 976–9

[53] Singer W and Gray C M 1995 Visual feature integration and the temporal correlation hypothesis *Ann. Rev. Neurosci.* 555–86

[54] Sik A, Penttonen M, Ylinen A and Buzsáki G 1995 Hippocampal CA1 interneurons: An *in vivo* intracellular labelling study *J. Neurosci.* **15** 6651–65

[55] Zhang S, Tiesinga P H E and José J V 2000 Model of carbachol-induced gamma-frequency oscillations in hippocampus *Proc. CNS'99*